Trapped Particle Effects in the Parametric Instability of Near-Acoustic Plasma Waves

M. Affolter,[1] F. Anderegg,[1] D. H. E. Dubin,[1] F. Valentini,[2] and C. F. Driscoll[1]
[1]Department of Physics, University of California at San Diego, La Jolla, California 92093, USA
[2]Dipartimento di Fisica, Università della Calabria, I-87036 Rende (CS), Italy

(Received 11 August 2018; revised manuscript received 13 October 2018; published 5 December 2018)

Quantitative experiments on the parametric decay instability of near-acoustic plasma waves provide strong evidence that trapped particles reduce the instability threshold below fluid models. At low temperatures, the broad characteristics of the parametric instability are determined by the frequency detuning of the pump and daughter wave, and the wave-wave coupling strength, surprisingly consistent with cold fluid, three-wave theories. However, at higher temperatures, trapped particle effects dominate, and the pump wave becomes unstable at half the threshold pump wave amplitude with similar exponential growth rates as for a cold plasma.

DOI: 10.1103/PhysRevLett.121.235004

The parametric instability is a fundamental nonlinear process occurring in a wide range of physical systems from solids to liquids to plasmas. Typically, three-wave couplings are used to predict instability rates, but systems with near-acoustic wave dispersion exhibit surprisingly stable soliton and cnoidal wave-train solutions in the continuum limit [1,2]. In plasmas, the parametric instability has been widely investigated theoretically [3–8], and it has been observed in tokamaks [9–12], non-neutral plasmas [13–15], high-intensity laser experiments [16,17], and other devices [18,19]. The parametric decay of ion acoustic waves (IAWs) has been postulated [20–24] as a possible cause for the saturation of stimulated Brillouin scattering observed in high-intensity laser experiments [16,17,25–28]. In those experiments, the IAWs are highly kinetic with a thermal velocity $\bar{v}$ near the phase velocity v_ϕ. However, quantitative measurements are lacking on the stability of near-acoustic waves and the influence of kinetic effects on this stability.

Here we measure the parametric decay instability of near-acoustic plasma waves in a quiescent ion column. These waves are azimuthally symmetric standing waves discretized by the axial wave number $k_z = m_z(\pi/L_p)$. We investigate the parametric decay of a large amplitude $m_z = 2$ pump wave to a longer wavelength $m_z = 1$ daughter wave, with linear dispersion giving weak detuning $\Delta\omega \equiv 2\omega_1 - \omega_2$.

Classical three-wave fluid theory [29,30] predicts exponential growth of the daughter wave amplitude A_1 above a temperature-independent threshold. However, a more complete multiharmonic fluid analysis [31] shows general stabilization, and experiments observe exponential instability with increasing temperature and wave amplitude, in broad correspondence with simulations and a new kinetic theory [32]. The experiments consistently observe three different regimes with decreasing pump wave amplitude: (1) strong exponential growth of the daughter wave at rates similar to three-wave coupling theory, (2) slow growth of the daughter wave superimposed on amplitude cycling, probably due to plasma heating, and (3) stable cyclic oscillations of the daughter wave amplitude, quantitatively consistent with the classical three-wave coupling strength.

The new kinetic theory [32] treats wave-particle trapping in the Vlasov continuum framework, and instability arises from the "negative dynamical compressibility" of a small distribution of particles weakly trapped between solitonlike wave peaks. This novel instability mechanism applies to low-collisionality plasmas supporting waves with nearly-acoustic dispersion relations such as IAWs, magnetized Langmuir waves, and Alfven waves. Simulations show that instability ceases if trapped particles are artificially removed, and the experimentally observed "slow oscillatory growth" regime is interpreted by this new theory as an increasing number of particles at the wave-trapping velocity. Varying the plasma temperature in the experiments and simulations results in instability at lower pump amplitudes as expected from trapped particle effects.

The experiments are performed on unneutralized Mg^+ ion plasmas confined in a Penning-Malmberg trap. These plasmas are in a near thermal equilibrium state described by rigid rotation and a top-hat density profile. Laser diagnostics [33] enable radial profiles of the plasma, giving the plasma radius $R_p \sim 0.5$ cm, an ion density $n_0 \sim 2 \times 10^7$ cm^{-3}, an on axis plasma length $12.4 \lesssim L_p \lesssim 20.3$ cm, and an average radial temperature T. The temperature is controlled over a range $10^{-3} \lesssim T \lesssim 0.62$ eV through laser cooling and cyclotron heating on $^{24}Mg^+$.

In these bounded plasmas, the dispersion relation of Langmuir waves is near acoustic because of the shielding from the radial boundary at $R_w = 2.86$ cm. The Trivelpiece-Gould (TG) dispersion relation [34] for periodic waves on an infinite-length column is

$$\omega(k_z) = \omega_p \frac{k_z}{\sqrt{k_z^2 + k_\perp^2}} \left[1 + \frac{3}{2}\left(\frac{\bar{v}}{v_\phi}\right)^2\right], \qquad (1)$$

where $k_z = m_z(\pi/L_p)$ and ω_p is the plasma frequency. The transverse wave number $k_\perp$ is determined by the boundary condition that the radial wave potential be continuous at the plasma radius [34]. For our R_w, this approximately determines $k_\perp \sim 0.9R_p^{-1} + 0.5k_z$.

The wave phase velocity $v_\phi \equiv \omega/k_z$ can be large compared to the thermal velocity $\bar{v} \equiv (T/m)^{1/2}$, here ranging over $90 \gtrsim v_\phi/\bar{v} \gtrsim 3.5$. The waves are excited from a cylindrical electrode near the plasma end, and the resulting charge density perturbation $|A_m|$ is detected as a voltage V_w on a separate electrode, as shown in the Fig. 1 inset. Gauss's Law directly relates the measured V_w to $|A_m|$ [35], where the linear density eigenfunction of these standing waves is

$$\Psi_m = \frac{1}{2} A_m(\tau) n_0 e^{-i\omega_m t} \cos(k_z z) J_0(k_\perp r) + \text{c.c.} \qquad (2)$$

for a top-hat density profile. Typically, a 40 cycle, amplitude-rounded sine wave burst excites the pump wave A_2, and the received mode amplitudes are obtained by fitting the digitized wall signal. The largest bursts generally heat the plasma by $\Delta T \sim 10^{-2}$ eV, and non-Maxwellian energetic tails may be generated below the 1% detection sensitivity of the laser velocity diagnostics.

Figure 1 shows frequency measurements of linear ($|A_m| \lesssim 1\%$) TG modes on cold plasmas for two different plasma lengths. Increasing the plasma length decreases the mode frequencies $23.8 \gtrsim \omega_1/2\pi \gtrsim 13.65$ kHz, and it decreases the relative detunings $3.1 \gtrsim \Delta\omega/2\pi \gtrsim 0.85$ kHz.

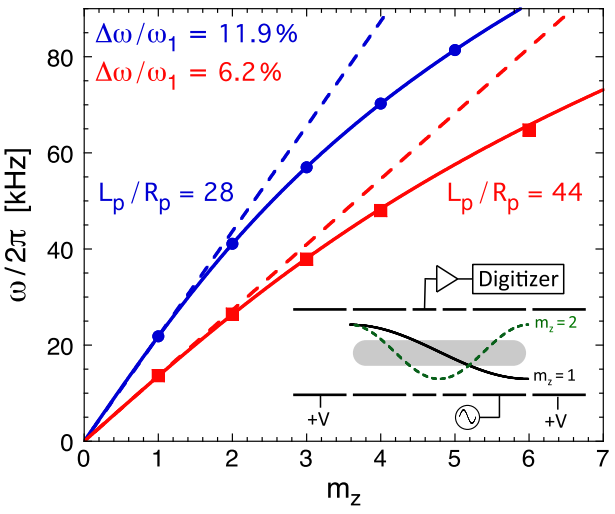

FIG. 1. Measured frequencies of standing TG waves (symbols) for two different plasma lengths on very cold plasmas with $T \sim 10^{-3}$ eV and $v_\phi/\bar{v} \sim 90$. Solid curves are one parameter fits to Eq. (1).

The solid curves are one-parameter fits to Eq. (1) with the plasma length as the fit parameter.

Shown in Fig. 2 are the three types of daughter wave evolutions observed in the experiments: exponential parametric decay, slow average growth, and detuned amplitude oscillations. Each plot corresponds to a different burst and resulting pump wave amplitude (arrows). Here, in addition to driving the $m_z = 2$ pump wave, we have used a concurrent 5% seed burst to excite the $m_z = 1$ daughter wave above the noise floor.

The pump wave amplitude directly determines a nonlinear wave-wave coupling rate defined as $\Gamma_0 \equiv |A_2|\omega_1(3R/8)$, where $R \sim 0.85$ is a geometric coupling coefficient. For large pump waves ($|A_2| \gtrsim 25\%$, $\Gamma_0/\Delta\omega \gtrsim 0.7$), Fig. 2(a) shows the parametric instability. Initially, the daughter wave amplitude grows exponentially at a rate $\Gamma_E = 8400\ \text{s}^{-1}$, phase-locked with the pump wave. Here, $A_m(\tau) \equiv |A_m(\tau)| \exp(i\theta_m(\tau))$, and we observe $\Delta\theta \equiv 2\theta_1 - \theta_2 = -0.75\pi$ during the exponential growth phase, consistent with simple three-wave coupling theory. When $A_1^{\max} \sim 0.7A_2^{\max}$, the direction of energy exchange reverses, and the pump and daughter wave amplitudes proceed to oscillate as the waves exchange energy back and forth. At this low temperature $T \sim 10^{-2}$ eV, the wave energy is

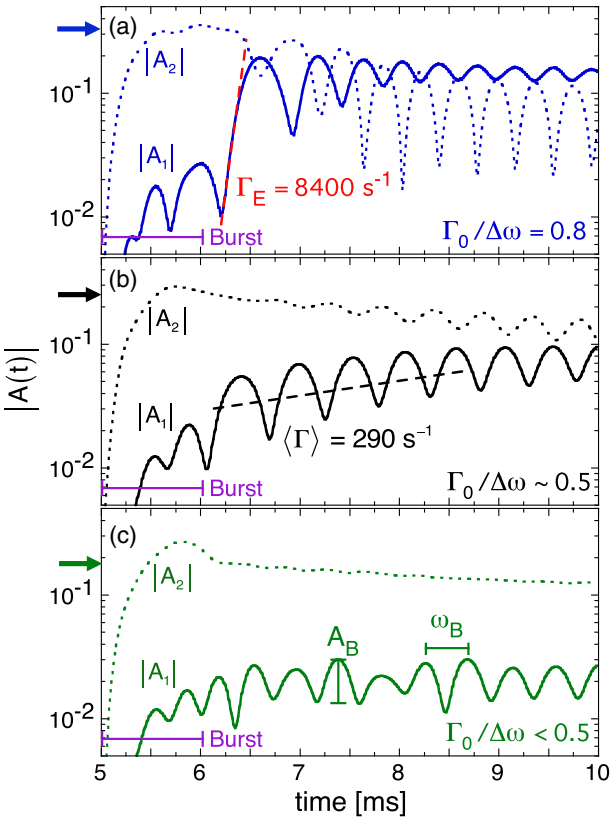

FIG. 2. Amplitude evolution of the $m_z = 1$ mode (solid) for three marginally different $m_z = 2$ amplitudes (dashed) on a plasma with $\Delta\omega/\omega_1 = 11.6\%$ and $T \sim 10^{-2}$ eV.

eventually dissipated by interspecies collisional drag [36] at a rate $\gamma \sim 50\ \mathrm{s}^{-1}$.

For moderate pump amplitudes ($20\% \lesssim |A_2| \lesssim 25\%$), we typically observe a slow average growth of the bouncing $m_z = 1$ wave, as shown in Fig. 2(b). This slow average growth rate $\langle\Gamma\rangle \lesssim 500\ \mathrm{s}^{-1}$ is not predicted by fluid theories. However, RZ kinetic particle-in-cell (PIC) simulations show a similar behavior as particles slowly become trapped in the wave potential.

In contrast, for small wave amplitudes ($|A_2| \lesssim 20\%$, $\Gamma_0/\Delta\omega \lesssim 0.5$), Fig. 2(c) shows that the pump wave is stable. On average the $m_z = 1$ mode amplitude remains constant with small excursions $A_B \propto |A_2|$ with a cycling rate $\omega_B \sim \Delta\omega$. This amplitude modulation is a result of the daughter wave being driven in-and-out of phase by the pump wave.

Fluid theory [29] characterizes this instability by two parameters: the scaled pump amplitude Γ_0 and frequency detuning $\Delta\omega$. This theory keeps the nonlinear terms in the fluid equations, and it uses a two time scale analysis for the density perturbation

$$\delta n = \Psi_1(r,z,t) + \Psi_2(r,z,t). \tag{3}$$

This gives the coupled amplitude equations

$$\begin{aligned} \dot{A}_1 &= -iXA_2A_1^* e^{i\Delta\omega t}, \\ \dot{A}_2 &= -iX(A_1)^2 e^{-i\Delta\omega t}, \end{aligned} \tag{4}$$

where $X = \Gamma_0/|A_2| = (3R/8)\omega_1$ is the nonlinear coupling coefficient. Solving these coupled equations, assuming $A_2 \gg A_1$ so that $\dot{A}_2 \approx 0$, we find

$$A_1(t) = \alpha e^{(\Gamma + i\Delta\omega/2)t} + \beta e^{-(\Gamma - i\Delta\omega/2)t}, \tag{5}$$

where $\Gamma = \sqrt{\Gamma_0^2 - (\Delta\omega/2)^2}$, and the constants α and β are constrained by Eq. (4).

Two different behaviors of the $m_z = 1$ amplitude are predicted by Eq. (5). For $\Gamma_0 > \Delta\omega/2$, Γ is real, and the daughter wave amplitude is comprised of an exponentially growing and decaying solution. This predicts the exponential growth rate $\Gamma_E = \Gamma$ of Fig. 2(a). In contrast, for $\Gamma_0 < \Delta\omega/2$, Γ is imaginary, and the daughter wave amplitude oscillates, as shown in Fig. 2(c), with an amplitude $A_B = \Gamma_0\langle A_1\rangle/(|\Gamma| + \Delta\omega/2)$, determined from α and β, and frequency $\omega_B = 2|\Gamma|$. This predicts the oscillatory coupling rate

$$\Gamma_{\mathrm{OCR}} \equiv \frac{A_B}{\langle A_1\rangle}\omega_B = \Gamma_0 \frac{2|\Gamma|}{|\Gamma| + \Delta\omega/2}. \tag{6}$$

Figure 3 plots both Γ_{OCR} and Γ_E at low temperatures $T \sim 10^{-2}$ eV versus the pump wave amplitude $|A_2|$ scaled by $\Delta\omega/\omega_1$ for a 2× range of plasma lengths and consequent $\Delta\omega/\omega_1$. The fluid prediction depends only on

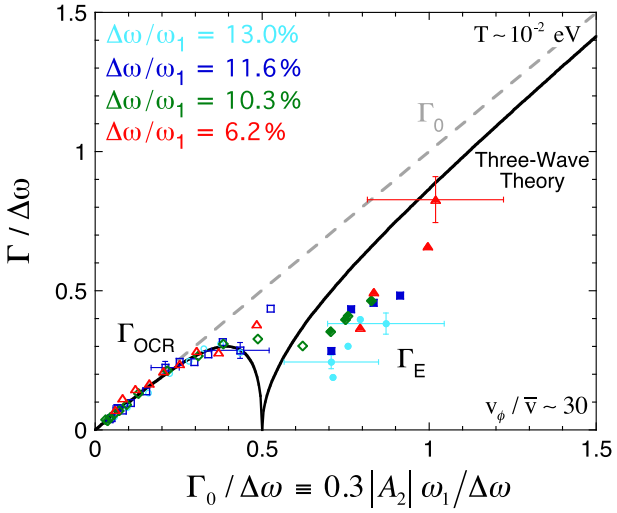

FIG. 3. Measurements of the oscillatory coupling (open symbols) and exponential growth (closed symbols) rates normalized to $\Delta\omega$ versus the scaled pump wave amplitude for various $\Delta\omega/\omega_1$. Solid black curve is three-wave theory.

$\Gamma_0/\Delta\omega \propto \omega_1/\Delta\omega$, so the $\Delta\omega/\omega_1$ scaling enables all data to be on the same axis. For $\Gamma_0/\Delta\omega < 0.4$, the measured Γ_{OCR} (open symbols) is in quantitative agreement with three-wave theory (solid curve) independent of $\Delta\omega/\omega_1$. For $\Gamma_0/\Delta\omega > 0.5$, the measured exponentiation rates Γ_E (solid symbols) are 10% to 50% lower than the three-wave fluid coupling prediction. Here, the daughter wave grows out of noise with a relative phase $\Delta\theta \sim -\arccos(\Delta\omega/2\Gamma_0)$, and the rate of this exponential growth is measured by fitting an exponentially growing sine wave to the digitized wall signal. In general, the rates $\Gamma_E \sim 3000$–$9000\ \mathrm{s}^{-1}$ are obtained from fits over 5–10 cycles of the growing $m_z = 1$ wave, and during this growth, the $m_z = 2$ amplitude is about 20 times the $m_z = 1$ amplitude. For $\Gamma_0/\Delta\omega \sim 0.5$, the experimental data is ambiguous, often showing slow growth, as in Fig. 2(b). The 20% horizontal error bars of Fig. 3 reflect systematic errors in the conversion of the wave induced voltage on a ring V_w to the density perturbation $|A_2|$. The 10% vertical error bars reflect our confidence in the amplitude fits.

This qualitative correspondence between cold fluid theory and measured Γ_E becomes untenable when the fluid analysis is extended to include nonlinear wave harmonics. For near-acoustic dispersion relations, the pump and daughter waves are not single sinusoidal oscillations as three-wave theory assumes, but instead, they contain multiple space and time harmonics of the fundamental waves. When these harmonics are included in the instability analysis, fluid theory [31] predicts that all of the traveling wave eigenmodes of this near-acoustic dispersion relation are stable to small perturbations, analogous to the stability of solitary-wave solutions of the Korteweg-de Vries [37] and Boussinesq [38] equations. In contrast, for the standing waves of interest in these experiments, the

instability is predicted [31] to be greatly suppressed but not eliminated by the addition of wave harmonics.

Experiments on warm plasmas further highlight the disparity from cold fluid theory. Figure 4(a) shows measurements of the decay instability at four different temperatures with fixed $\Delta\omega/\omega_1 \sim 11\%$. At low temperatures ($v_\phi/\bar{v} \gtrsim 5$), the instability threshold is roughly determined by $\Gamma_0/\Delta\omega \sim 0.6$. In contrast, for a plasma with $v_\phi/\bar{v} \sim 3.5$, we observe similar exponential growth rates as for a cold plasma, but at half the pump wave amplitude, i.e., $\Gamma_0/\Delta\omega \sim 0.3$. Previous qualitative experiments [15] were suggestive of a temperature dependent instability threshold, and early experiments reported by us [39] missed this temperature dependence, as those experiments were conducted in a regime ($\Delta\omega/\omega_1 \sim 18\%$ and a strong $m_z = 1$ seed) in which the transition from oscillatory coupling to exponential growth was strongly obfuscated by the slow average growth regime.

At these higher temperatures ($3.5 \lesssim v_\phi/\bar{v} \lesssim 5$), particles become trapped even at relatively small wave amplitudes. Although this trapped particle fraction is below the sensitivity for direct laser diagnostics, they are indirectly observed through nonlinear Landau damping. Small amplitude waves ($|A_m| \lesssim 0.1\%$) damp at the linear Landau rate $8000 \gtrsim \gamma_L \gtrsim 50\ \mathrm{s}^{-1}$ [36]. Whereas, at larger wave amplitudes, these resonant particles are trapped in the wave potential resulting in trapping oscillations at a frequency

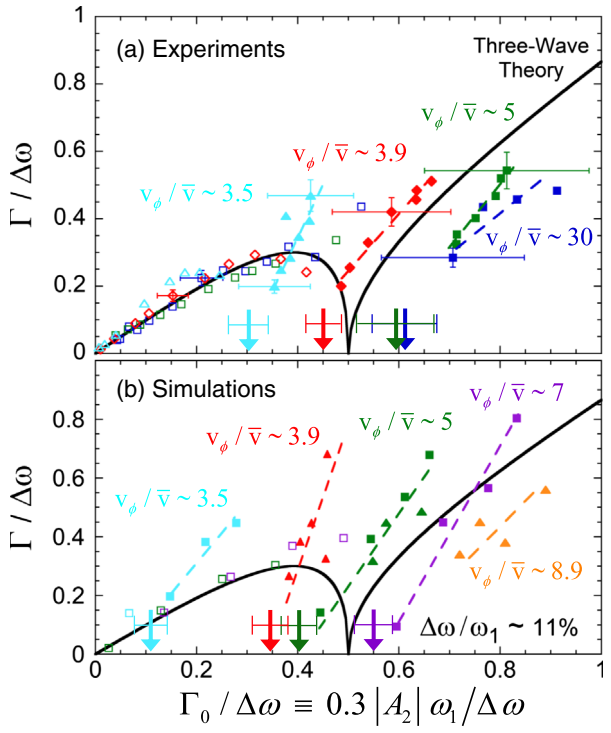

FIG. 4. Measurements (a) and simulations (b) of OCR and exponential growth rates at different plasma temperatures. The reduction in the instability threshold (arrows) at lower $v_\phi/\bar{v}$ contradicts fluid theories.

$\omega_T^2 \sim |A_m|\omega^2$, and diminishing the damping rate as the trapped particles phase mix [40]. The large amplitude kinetic pump waves of Fig. 4(a) have weak damping $\gamma \sim 100\ \mathrm{s}^{-1}$, presumably resulting from collisional repopulation of the plateau in the velocity distribution.

The observed reduction in the instability threshold of Fig. 4(a) is inconsistent with fluid theories, but it is in qualitative agreement with a new kinetic theory [32], which predicts exponential growth rates similar to the experiments as due to a small fraction of these wave-trapped particles. These trapped particles destabilize the wave because they exhibit negative compressibility. In the $2 \rightarrow 1$ instability, adjacent peaks of the wave train approach one another and therefore recede from the next peaks. From a fluid perspective, the density and pressure of particles trapped between approaching peaks would increase, and would decrease for particles trapped between receding peaks, producing a restoring force that stabilizes these modulations. Trapped particles with energies just below the approaching wave peaks, however, gain sufficient energy to become passing, and they are then retrapped between receding peaks. The net effect of these marginally trapped particles is to reverse the sign of the trapped particle density and pressure change, which produces a force that amplifies the modulation. The exponential instability occurs when the trapped particle fraction is sufficiently large, here estimated to be $f_T \gtrsim 0.1\%$. This trapped particle mechanism is a general phenomenon that could play a role in other nonlinear systems, such as nonlinear IAWs where kinetic simulations [22,41] show instability thresholds below fluid theory predictions.

To further support this trapped particle mechanism, z-periodic (r, z, v_z) drift-kinetic Poisson (squares) and finite-length, kinetic, RZ PIC (triangles) simulations of the experiments are conducted [Fig. 4(b)]. At the lowest temperatures achievable by these simulations ($v_\phi/\bar{v} \sim 8.9$), exponential growth rates consistent with the experiments are observed. However, it is the trapped particles in these simulations that cause the instability. If the trapped particle population is artificially eliminated, the instability ceases. At higher temperatures, the simulations predict a lower instability threshold than experimentally observed for a given $v_\phi/\bar{v}$, suggesting that the trapped particle fraction formed in these simulations is larger than that of the experiments. This discrepancy might be a result of collisions or multispecies effects, which are neglected in the simulations.

In summary, a small fraction of wave-trapped particles apparently destabilizes the pump wave, enabling the exponential growth of longer-wavelength waves. Experiments and simulations show stronger growth with increasing plasma temperature and decreasing $v_\phi/\bar{v}$. Incisively, the simulations show the cessation of instability when particles near v_ϕ are removed. Detailed measurements of the particle velocity distribution near v_ϕ will be required for a quantitative comparison to the new theory.

This work was supported by DOE-HEDLP Grant No. DE-SC0008693. M. A. was supported by the DOE FES Postdoctoral Research Program administered by ORISE for the DOE. ORISE is managed by ORAU under DOE Contract No. DE-SC0014664. F. V. was supported by Contract No. ASI-INAF 2015-039-R.O.

[1] J. A. Pava, *Nonlinear Dispersive Equations: Existence and Stability of Solitary and Periodic Travelling Wave Solutions* (American Mathematical Society, Providence, 2009), Vol. 156.
[2] A. Jeffrey and T. Kakutani, SIAM Rev. **14**, 582 (1972).
[3] R. Z. Sagdeev and A. A. Galeev, *Nonlinear Plasma Theory* (W. A. Benjamin, New York, 1969).
[4] R. N. Franklin, Rep. Prog. Phys. **40**, 1369 (1977).
[5] F. W. Perkins and J. Flick, Phys. Fluids **14**, 2012 (1971).
[6] M. N. Rosenbluth, Phys. Rev. Lett. **29**, 565 (1972).
[7] M. Porkolab, Fusion Eng. Des. **12**, 93 (1990).
[8] J. F. Drake, P. K. Kaw, Y. C. Lee, G. Schmid, C. S. Liu, and M. N. Rosenbluth, Phys. Fluids **17**, 778 (1974).
[9] M. Porkolab, S. Bernabei, W. M. Hooke, R. W. Motley, and T. Nagashima, Phys. Rev. Lett. **38**, 230 (1977).
[10] Y. Takase, M. Porkolab, J. J. Schuss, R. L. Watterson, C. L. Fiore, R. E. Slusher, and C. M. Surko, Phys. Fluids **28**, 983 (1985).
[11] S. Baek, R. Parker, S. Shiraiwa, G. Wallace, P. Bonoli, D. Brunner, I. Faust, A. Hubbard, B. LaBombard, and M. Porkolab, Plasma Phys. Controlled Fusion **55**, 052001 (2013).
[12] F. S. McDermott, G. Bekefi, K. E. Hackett, J. S. Levine, and M. Porkolab, Phys. Fluids **25**, 1488 (1982).
[13] A. A. Kabantsev, Y. A. Tsidulko, and C. F. Driscoll, Phys. Rev. Lett. **112**, 055003 (2014).
[14] A. A. Kabantsev, F. Valentini, and C. F. Driscoll, AIP Conf. Proc. **862**, 13 (2006).
[15] H. Higaki, Plasma Phys. Controlled Fusion **39**, 1793 (1997).
[16] H. C. Bandulet, C. Labaune, K. Lewis, and S. Depierreux, Phys. Rev. Lett. **93**, 035002 (2004).
[17] C. Niemann, S. H. Glenzer, J. Knight, L. Divol, E. A. Williams, G. Gregori, B. I. Cohen, C. Constantin, D. H. Froula, D. S. Montgomery, and R. P. Johnson, Phys. Rev. Lett. **93**, 045004 (2004).
[18] R. Stenzel and A. Y. Wong, Phys. Rev. Lett. **28**, 274 (1972).
[19] S. Dorfman and T. A. Carter, Phys. Rev. Lett. **116**, 195002 (2016).
[20] S. J. Karttunen, J. N. McMullin, and A. A. Offenberger, Phys. Fluids **24**, 447 (1981).
[21] B. I. Cohen, B. F. Lasinski, A. B. Langdon, and E. A. Williams, Phys. Plasmas **4**, 956 (1997).
[22] T. Chapman, S. Brunner, J. Banks, R. Berger, B. Cohen, and E. Williams, Phys. Plasmas **21**, 042107 (2014).
[23] D. Pesme, C. Riconda, and V. Tikhonchuk, Phys. Plasmas **12**, 092101 (2005).
[24] B. Cohen, E. Williams, R. Berger, D. Pesme, and C. Riconda, Phys. Plasmas **16**, 032701 (2009).
[25] A. Ng, L. Pitt, D. Salzmann, and A. A. Offenberger, Phys. Rev. Lett. **42**, 307 (1979).
[26] C. E. Clayton, C. Joshi, and F. F. Chen, Phys. Rev. Lett. **51**, 1656 (1983).
[27] J. E. Bernard and J. Meyer, Phys. Rev. Lett. **55**, 79 (1985).
[28] S. H. Glenzer, L. M. Divol, R. L. Berger, C. Geddes, R. K. Kirkwood, J. D. Moody, E. A. Williams, and P. E. Young, Phys. Rev. Lett. **86**, 2565 (2001).
[29] A. Ashourvan, Doctoral Dissertation, UCSD, 2014.
[30] J. A. Armstrong, N. Bloembergen, J. Ducuing, and P. S. Pershan, Phys. Rev. **127**, 1918 (1962).
[31] D. H. E. Dubin and A. Ashourvan, Phys. Plasmas **22**, 102102 (2015).
[32] D. H. E. Dubin, Phys. Rev. Lett. **121**, 015001 (2018).
[33] F. Anderegg, X.-P. Huang, E. Sarid, and C. Driscoll, Rev. Sci. Instrum. **68**, 2367 (1997).
[34] A. Trivelpiece and R. Gould, J. Appl. Phys. **30**, 1784 (1959).
[35] M. Affolter, F. Anderegg, D. H. E. Dubin, and C. F. Driscoll, Phys. Plasmas **25**, 055701 (2018).
[36] M. Affolter, F. Anderegg, D. H. E. Dubin, and C. F. Driscoll, Phys. Rev. Lett. **117**, 155001 (2016).
[37] T. B. Benjamin, Proc. R. Soc. A **328**, 153 (1972).
[38] J. L. Bona and R. L. Sachs, Commun. Math. Phys. **118**, 15 (1988).
[39] F. Anderegg, M. Affolter, A. Ashourvan, D. H. E. Dubin, F. Valentini, and C. F. Driscoll, AIP Conf. Proc. **1668**, 020001 (2015).
[40] J. R. Danielson, F. Anderegg, and C. F. Driscoll, Phys. Rev. Lett. **92**, 245003 (2004).
[41] T. Chapman, R. L. Berger, B. I. Cohen, J. W. Banks, and S. Brunner, Phys. Rev. Lett. **119**, 055002 (2017).